MAGNETOHYDRODYNAMIC FLOW OF POWELL-EYRING FLUID BY A STRETCHING CYLINDER WITH NEWTONIAN HEATING

by

Tasawar HAYAT [a,b]***, Zakir HUSSAIN*** [a*]***, Muhammad FAROOQ*** [c]***, and Ahmed ALSAEDI*** [b]

[a] Department of Mathematics, Quaid-I-Azam University, Islamabad, Pakistan
[b] Non-Linear Analysis and Applied Mathematics, Research Group, Department of Mathematics, Faculty of Science, King Abdulaziz University, Jeddah, Saudi Arabia
[c] Department of Mathematics, Riphah International University, Islamabad, Pakistan

Original scientific paper
https://doi.org/10.2298/TSCI150717162H

This paper examines MHD flow of Powell-Eyring fluid by a stretching cylinder with thermal radiation. Analysis has been presented through inclined magnetic field. Characteristics of heat transfer are analyzed with advanced boundary condition (i. e., Newtonian heating). Suitable transformations convert the non-linear PDE to the non-linear ODE. Convergent series solutions of momentum and energy equations are developed. Effects of different pertinent parameters on the velocity and temperature distributions are shown graphically. Numerical values of the skin friction coefficient and Nusselt number are also computed and analyzed. Comparison of the present study with the previous published work is also examined. Higher values of fluid, M, and curvature parameters show enhancement in the fluid velocity while opposite behavior is observed for Hartmann number and suction parameter. Conjugate and radiation parameters lead to an increase in temperature.

Key words: *stretching cylinder, MHD, thermal radiation, Powell-Eyring fluid, Newtonian heating*

Introduction

Analysis of non-Newtonian fluids is still of great interest to the researchers because these fluids are more appropriate in the industrial applications such as food engineering, power engineering, petroleum production, and in the industries of polymer solutions. Non-Newtonian fluids can not be described by a linear relationship between stress and rate of strain. Non-Newtonian fluids are more complex than the Newtonian fluids due to their diverse characteristics. Powell-Erying fluids [1] is one of the non-Newtonian fluids which has some advantages over the power law model *i. e.*: it is based on kinetic theory of liquids and at low and high shear rates it shows Newtonian behavior. Patel and Timol [2] studied numerical treatment of MHD Powell-Erying fluid flow using the asymptotic boundary conditions. Hayat *et al.* [3] examined radiative effects in 3-D flow of MHD Erying-Powel fluid. Ara *et al.* [4] studied radiation effect on boundary-layer flow of Erying-Powell fluid over an exponentially shrinking sheet. Boundary-layer stagnation point flow of Powell-Erying fluid with melting heat transfer was presented by Hayat *et al.* [5].

[*] Corresponding author, e-mail: zakir.qamar@yahoo.com

The MHD describes the mutual interaction of the magnetic fields and fluid flow. The MHD flows are discussed for the fluids which are electrically conducting and non-magnetic include strong electrolytes, liquid metals and hot ionized gases. The analysis of MHD flow is very important and has widespread applications in the areas of technology and engineering. Such flows appear in design cooling systems, MHD generators, electric motors, blood flow measurements, pumps and flow meters, *etc*. Ishak [6] discussed MHD boundary-layer flow due to an exponentially stretching sheet with radiation effect. Noor and Hashim [7] studied MHD flow and heat transfer adjacent to a permeable shrinking sheet embedded in a porous medium. Turkyilmazoglu [8] explored heat transfer characteristics in MHD flow induce by a shrinking rotating disk. Heat and mass transfer effects in MHD stagnation point flow of second grade fluid by a stretching cylinder was examined by Hayat *et al.* [9]. Sheikholeslami *et al*. [10] presented MHD boundary-layer flow of nanofluid using KKL model. Natural convection in MHD flow over a flat plate with convective condition was analyzed by Rashidi *et al.* [11].

Merkin [12] suggested four common ways of heat transfer from wall to ambient temperature distribution *i. e.*: constant or prescribed surface temperature, constant or prescribe surface flux, conjugate or convective boundary condition and Newtonian heating describing that the heat transfer from any material surface with a finite heat capacity is proportional to the local surface temperature. Newtonian heating phenomenon is especially important in practical applications such as to design heat exchanger, conjugate heat transfer around fins and also in convective flow. Ramzan *et al.* [13] explored the characteristics of MHD flow of couple stress fluid with Newtonian heating. Salleh and Nazar [14], Salleh *et al*. [15], Narahari and Dutta [16] discussed in detail about free convection boundary-layer flow of micropolar fluid due to solid sphere with Newtonian heating.

It has been analyzed from the literature survey that boundary-layer flow of non-Newtonian fluids over a stretching cylinder with Newtonian heating is not investigated yet. Therefore, our main object is to explore the radiative MHD flow of Powell-Eyring fluid over a stretching cylinder with Newtonian heating. Rosseland approximation is used to describe the radiative heat flux. A system of non-linear PDE is converted into the non-linear ODE. Homotopy analysis method (HAM) [17-35] is used to achieve the convergent series solutions of the momentum and energy equations. Behaviors of various pertinent parameters on the velocity and temperature distributions are analyzed through graphs. It is found that present analysis reduces to the flow over a flat plate for zero curvature. The HAM solutions are good than the numerical solutions in aspect of the following reasons.

Firstly HAM provides the solution within the domain of concern at each point while numerical solution controls only set of discrete points in the domain.

Secondly approximate solutions obtained by algebraically need less time and acceptable accuracy when compared with numerical solutions.

Thirdly most of the scientific packages although need a few initial guesses for the solutions are not convergent generally. In such cases approximate solutions can present improved initial guess that can be readily better to the exact numerical solution in few iterations. In short an approximate solution if it is analytical, is the most favorable than the numerical solutions.

Mathematical formulation

Consider the steady 2-D MHD flow of Powell-Eyring fluid due to a permeable stretching cylinder with Newtonian heating. The dissipation effects is not included in heat transfer process. Magnetic field is assumed in the inclined direction *i. e.*, makes an angle, ϕ, with the cylinder. Heat transfer is carried out with thermal radiation. Cylindrical co-ordinates are selected in such a way that z-axis is along the axial direction of stretching cylinder and r-axis normal to it.

Under the boundary-layer approximations, *i. e.*, $u = O(\delta)$, $r = O(\delta)$, $w = O(1)$ and $z = O(1)$, the continuity, momentum, and energy equations are expressed:

$$\frac{\partial(ru)}{\partial r}+\frac{\partial(rw)}{\partial z}=0 \tag{1}$$

$$u\frac{\partial w}{\partial r}+\omega\frac{\partial w}{\partial z} = \nu\left(\frac{\partial^2 w}{\partial r^2}+\frac{1}{r}\frac{\partial w}{\partial r}\right)+\frac{1}{\rho\beta c}\left(\frac{\partial^2 w}{\partial r^2}+\frac{1}{r}\frac{\partial w}{\partial r}\right)-$$
$$-\frac{1}{6\rho\beta c^3}\left[\frac{1}{r}\left(\frac{\partial w}{\partial r}\right)^3+3\left(\frac{\partial w}{\partial r}\right)^2\left(\frac{\partial^2 w}{\partial r^2}\right)\right]-\frac{\sigma\beta_0^2}{\rho}\sin^2\phi u \tag{2}$$

$$u\frac{\partial T}{\partial r}+w\frac{\partial T}{\partial z}=\frac{k}{\rho c_\rho}\left(\frac{\partial^2 T}{\partial r^2}+\frac{1}{r}\frac{\partial T}{\partial r}\right)+\frac{16\sigma^* T_\infty^3}{3k^*\rho c_\rho}\left(\frac{\partial^2 T}{\partial r^2}+\frac{1}{r}\frac{\partial T}{\partial r}\right) \tag{3}$$

subject to the boundary conditions:

$$w=w_e=\frac{U_0 z}{l},\quad u=-u_w,\quad \frac{\partial T}{\partial r}=-h_s T \quad \text{at} \quad r=R^*,\quad w\to 0,\quad T\to T_\infty,\quad \text{as} \quad r\to\infty \tag{4}$$

where u and w denote the velocity components in the r- and z-directions, respectively, u_W – represents the suction ($u_W > 0$) or injection ($u_W < 0$), U_0 – the reference velocity, l – the characteristic length, ν – the kinematic viscosity, ρ – the density, β and c – the fluid parameters, c_P – the specific heat, k – the thermal conductivity, ϕ – the angle of inclination of permeable cylinder, $\sigma^*$and k^* – the Stefan-Boltzman constant and Rosseland mean absorption coefficient, respectively, σ – electric charge density, β_0 – the strength of magnetic field, h_S – heat transfer coefficient, T and T_∞ – the temperatures of the fluid and surrounding, respectively, and w_e – the stretching velocity. The results for magnetic field in transverse direction is obtained when $\phi = \pi/2$. Using the transformations of the form:

$$\eta=\sqrt{\frac{U_0}{\nu l}}\left(\frac{r^2-R^{*2}}{2R^*}\right),\quad w=\frac{U_0 z}{l}f'(\eta),\quad u=-\sqrt{\frac{\nu U_0}{l}}\frac{R^*}{r}f(\eta),\quad \theta(\eta)=\frac{T-T_\infty}{T_\infty} \tag{5}$$

the equation of incompressibility is identically satisfied while eqs. (2) and (3) are reduced to:

$$(1+2\gamma\eta)(1+M)f'''+ff''-(f')^2+2\gamma(1+M)f''-\frac{4}{3}(1+2\gamma\eta)M\gamma\lambda(f'')^3-$$
$$-(1+2\gamma\eta)^2\lambda M f''^2 f'''-\mathrm{K}^2\sin^2\phi f'=0 \tag{6}$$

$$(1+2\gamma\eta)\left(1+\frac{4R}{3}\right)\theta''+2\left(1+\frac{4R}{3}\right)\gamma\theta'+\Pr f\theta'=0 \tag{7}$$

$$f(0)=S,\quad f'(0)=1,\quad \theta'(0)=-\alpha[1+\theta(0)]\quad f'(\infty)=0,\quad \theta(\infty)=0 \tag{8}$$

where γ is the curvature parameter, M and λ – the fluid parameters, R – the radiation parameter, K^2 – the Hartmann number, Pr – the Prandtl number, α – the conjugate parameter for Newtonian heating, and S – the suction/injection parameter. The definitions of these parameters are:

$$\gamma=\sqrt{\frac{\nu l}{U_0 R^{*2}}},\quad \Pr=\frac{\mu c_p}{k},\quad M=\frac{1}{\mu\beta c},\quad \lambda=\frac{U_0^3 z^2}{2l^3c^2\nu},\quad \mathrm{K}^2=\frac{\sigma\beta_0^2 l}{\rho U_0},\quad R=\frac{4\sigma^* T_\infty^3}{k^* k},\quad S=u_w\sqrt{\frac{l}{\nu U_o'}},\quad \alpha=h_s\sqrt{\frac{\nu}{U_0}}l \tag{9}$$

Skin friction coefficient and local Nusselt number can be defined:

$$C_f=\frac{\tau_{rz}}{\rho w_e^2},\qquad \mathrm{Nu_z}=\frac{zq_w}{k(T-T_\infty)}$$
$$\tau_w=\left[\left(\mu+\frac{1}{\beta c}\right)\left(\frac{\partial w}{\partial r}\right)-\frac{1}{6\beta c^3}\left(\frac{\partial w}{\partial r}\right)^3\right]_{r=R^*},\qquad q_w=-\left(k+\frac{16\sigma^* T\infty^3}{3k^*}\right)\left(\frac{\partial T}{\partial r}\right)_{r=R^*} \tag{10}$$

Dimensionless forms of skin friction and local Nusselt number are:

$$Cf\sqrt{\mathrm{Re}_z}=(1+M)f''(0)-\frac{\lambda}{3}M\left[f''(0)\right]^3,\qquad \mathrm{Nu}_z\mathrm{Re}_z^{-1/2}=\alpha\left(1+\frac{4R}{3}\right)\left[1+\frac{1}{\theta(0)}\right] \tag{11}$$

where $\mathrm{Re}_z = w_{ez}/\nu$ is the local Reynolds number.

Homotopic solutions

To find the series solutions of the governing equations by HAM, it is necessary to have the initial guesses (f_0, θ_0) which satisfy the given boundary conditions and the linear operators ($\mathcal{L}_f$, $\mathcal{L}_\theta$). The initial guesses and linear operators are taken:

$$f_0(\eta)=S+[1-\exp(-\eta)],\qquad \theta_0(\eta)=\left(\frac{\alpha}{1-\alpha}\right)\exp(-\eta) \tag{12}$$

$$\mathcal{L}_f(\eta)=\frac{\mathrm{d}^3 f}{\mathrm{d}\eta^3}-\frac{\mathrm{d}f}{\mathrm{d}\eta},\qquad \mathcal{L}_\theta(\eta)=\frac{\mathrm{d}^2\theta}{\mathrm{d}\eta^2}-\theta \tag{13}$$

Convergence analysis

Convergence region is of great importance for acquiring the series solutions. In these series solutions there is a vast opportunity to select the value of the auxiliary parameter $\hbar$ which confirms the convergence region. Therefore, we have plotted the $\hbar$-curves in figs. 1 and 2. Here the admissible ranges of the auxiliary parameters $\hbar_f$ and $\hbar_\theta$ are $-1.6 \leq \hbar_f \leq -0.5$ and $-1.3 \leq \hbar_\theta \leq -2.5$.

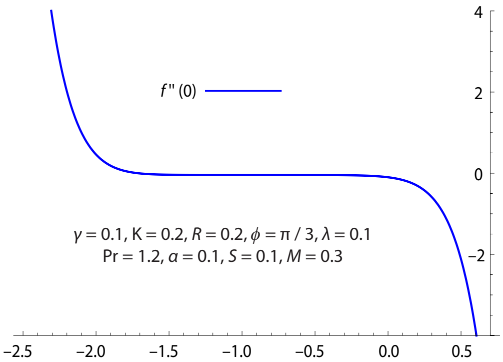

Figure 1. The $\hbar$− curve for $f(\eta)$

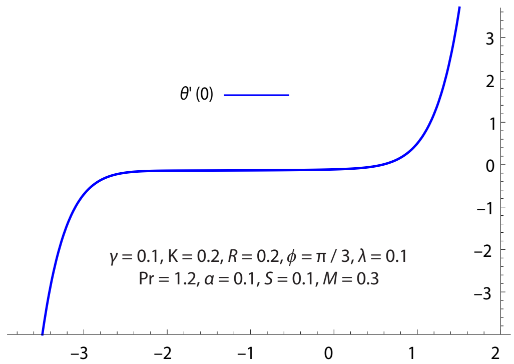

Figure 2. The $\hbar$ − curve for $\theta(\eta)$

Discussion

Theme of this section is to analyze the effects of various parameters on the velocity and temperature profiles. Figure 3 is plotted for the effect of Hartmann number on the velocity profile. It is noted that velocity and boundary-layer thickness decrease for higher values of Hartman number. Infact higher values of Hartmann number results in the enhancement of Lorentz force which provides resistance to fluid motion and consequently the velocity profile decreases. Figure 4 is sketched for the influence of Hartmann number on the temperature distribution. It is observed that temperature distribution increases for larger values of Hartmann number.

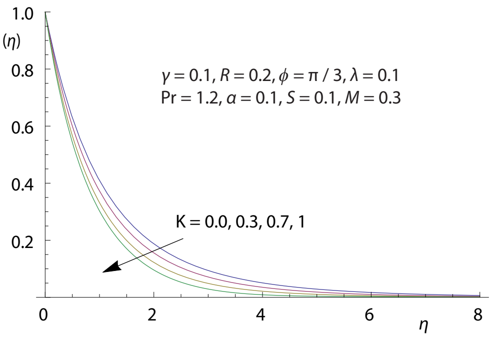

Figure 3. Influence of K on $f'(\eta)$

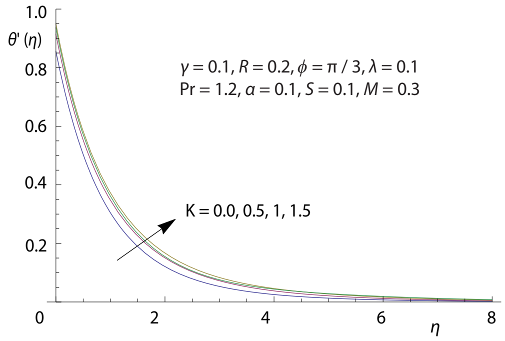

Figure 4. Influence of K on $\theta(\eta)$

Figure 5 shows the behavior of curvature parameter on velocity profile. It is concluded that as the values of γ increase the velocity profile decreases near the surface and it increases away from the cylinder. In fact when the value of curvature parameter increases then radius of the cylinder decreases. Thus contact area of the cylinder with the fluid decreases and offers less resistance to the fluid motion. Hence velocity profile increases. Behavior of curvature parameter on temperature profile is analyzed in fig. 6. Temperature distribution decreases near the surface of cylinder while it increases away from the surface. Through increase of curvature parameter the radius of cylinder decreases which results in the reduction of conduction of heat process near the surface while it enhances the convection heat transfer away from the the surface. Therefore, temperature first decreases and then increases.

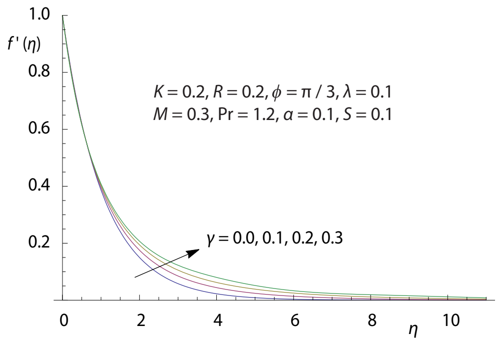

Figure 5. Influence of γ on $f'(\eta)$

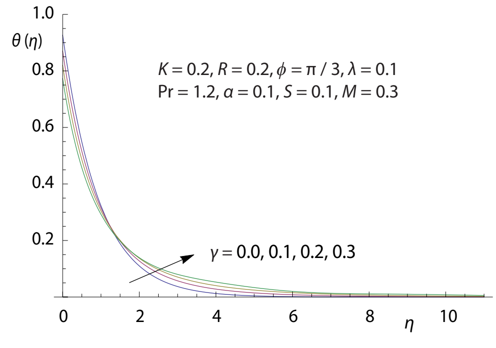

Figure 6. Influence of γ on $\theta(\eta)$

Influence of angle of inclination on velocity profile is displayed in fig. 7. Velocity profile is higher for larger values of ϕ. In fact higher values of ϕ correspond to larger magnetic field. Figure 8 is sketched for the variations of angle of inclination ϕ on temperature profile. It is concluded that temperature profile enhances for larger values of ϕ. Because the values of ϕ correspond to strong magnetic field and Lorentz force. So temperature profile increases.

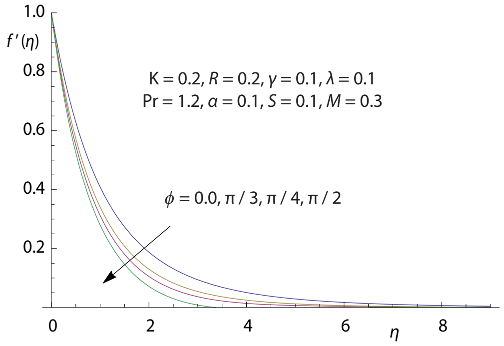

Figure 7. Influence of ϕ on $f'(\eta)$

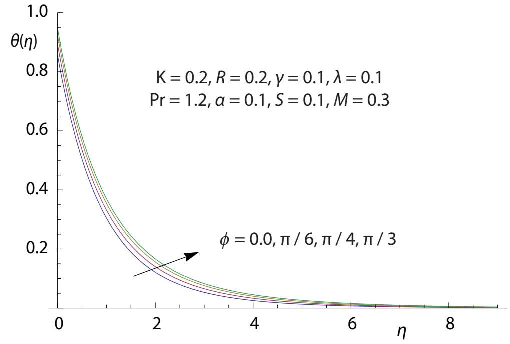

Figure 8. Influence of ϕ on θ (η)

Figure 9 provides the analysis for the effects of fluid parameter, M, on the velocity profile. It is seen that velocity profile and boundary-layer thickness increase with an increase in fluid parameter M. In fact for higher values of M the viscosity of the fluid tends to decrease which is responsible for the enhancement of velocity profile. Characteristics of fluid parameter M on temperature profile is presented in fig. 10. It is concluded that higher values of M result in the reduction of temperature profile. Further thermal boundary-layer thickness also decreases. It is due to the fact that viscosity of the fluid decreases as fluid parameter M increases.

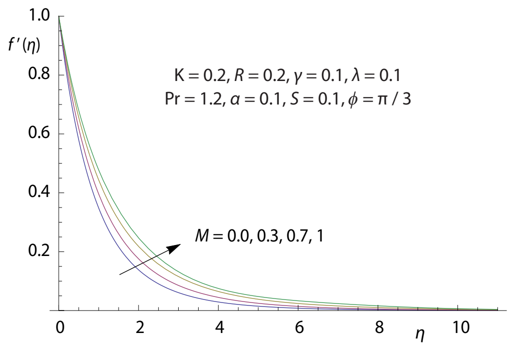

Figure 9. Influence of M on f′ (η)

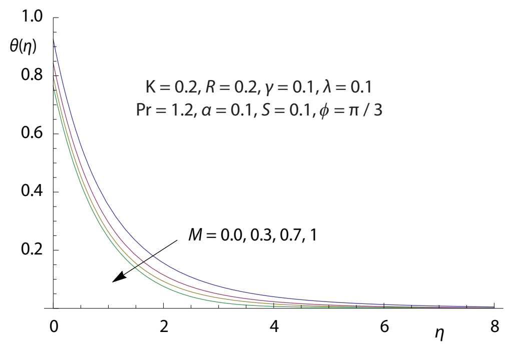

Figure 10. Influence of M on θ (η)

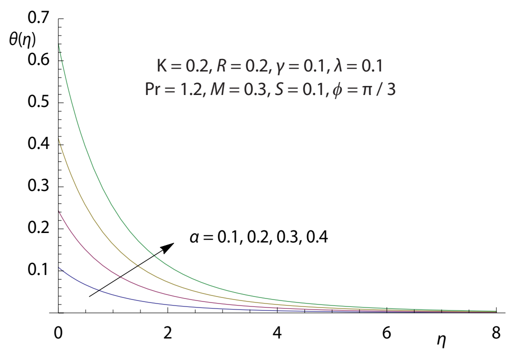

Figure 11. Influence of α on θ (η)

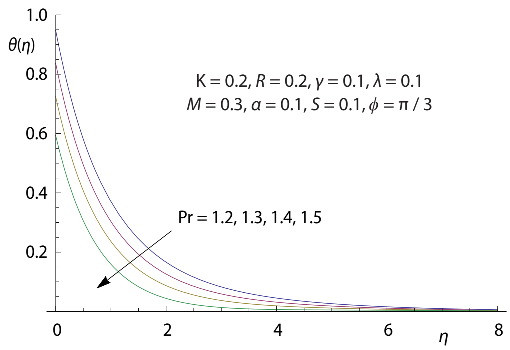

Figure 12. Influence of Prandtl number on θ (η)

Therefore temperature profile decreases. Influence of conjugate parameter, α, on temperature distribution is displayed in fig. 11. It is depicted that temperature distribution is higher for larger values of conjugate parameter α. Further thermal boundary-layer thickness also increases with an increase in conjugate parameter heat transfer coefficient which results in the enhancement of temperature profile. Figure 12 shows the behavior of Prandtl number on temperature distribution. It is concluded that temperature distribution and thermal boundary-layer thickness decrease with an increase in Prandtl number. It relates the momentum diffusivity to thermal diffusivity. Hence higher Prandtl number corresponds to lower thermal diffusivity and ultimate the temperature distribution decreases. Variation of suction parameter, S, on velocity and temperature profiles are sketched in the figs. 13 and 14, respectively. It is analyzed that both velocity and temperature profiles decrease with increase in suction parameter. Behavior of radiation parameter, R, on temperature profile is illustrated in the fig. 15. Temperature and the associated boundary-layer thickness increase for larger values of radiation parameter. Here higher values of radiation parameter result in the reduction of mean absorption coefficient and thus the temperature profile increases.

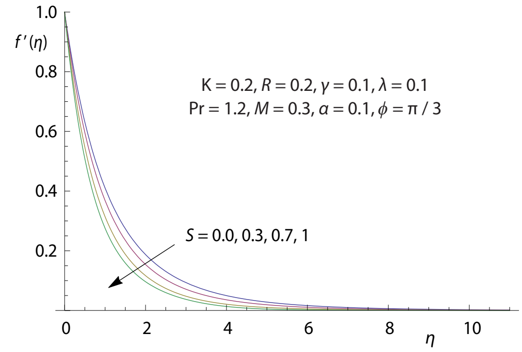

Figure 13. Influence of S on $f'(\eta)$

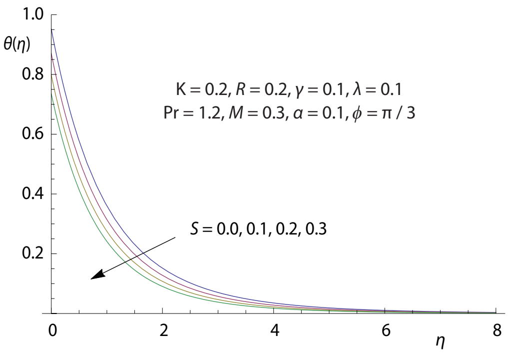

Figure 14. Influence of S on $\theta(\eta)$

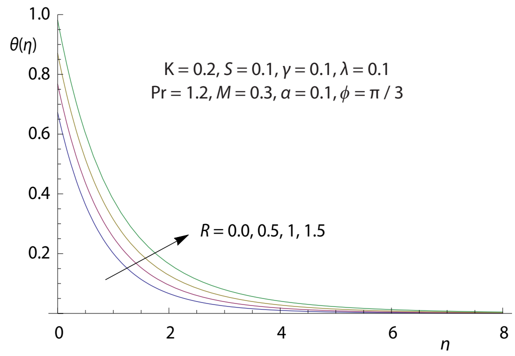

Figure 15. Influence of R on $\theta(\eta)$

Table 1 shows the convergence of the series solutions for the governing momentum and energy equations. It is observed that 15th and 20th order of approximations are sufficient for the convergence of momentum and energy equations. Table 2 represents the numerical values of $f''(0)$ with the previous results in the limiting case when $\gamma = 0$, $\mathrm{K} = 0$, and $S = 0$. It is concluded that both the results are in good agreement. Table 3 presents the comparison of skin friction coefficient with the previous published work [36] when $\gamma = \mathrm{K} = S = 0$. It is evident that both the results are in good agreement. Skin friction coefficient increases with an increase in M and it decreases with λ. Therefore, small values of M and large values of λ can be used for the reduction of skin friction coefficient. Table 4 presents the numerical values of skin friction for various parameters. It is concluded that skin friction increases for larger curvature parameter γ and Hartmann number, K^2, and it decreases with increase in the values of fluid parameter M. Table 5 depicts the numerical values of Nusselt number for various parameters. It is

Table 1. Convergence of the series solutions for different order of approximations when $\gamma = 0.1$, $\lambda = 0.1$, $M = 0.3$, K = 0.1, $S = 0.1$, $R = 0.2$, $\phi = \pi/3$, $\alpha = 0.1$, and Pr = 1.2

Order of approximations	$-f''(0)$	$-\theta'(0)$
1	0.0552	0.1167
5	0.0434	0.1277
10	0.0412	0.1355
15	0.0409	0.1401
20	0.0409	0.1408
25	0.0409	0.1408

concluded that Nusselt number increases with the increase of curvature parameter, γ, fluid parameter, M, conjugate parameter α. suction/injection parameter, S, and Prandtl number while it decrease with fluid parameter, λ, inclination angle, ϕ, Hartmann number, K^2, and radiation parameter, R. As rate of heat transfer is high for large values of curvature parameter γ and fluid parameter M, so these parameters can be used as coolant agent. Thus it is concluded that cylindrical shape devices with large curvature *i. e*, with small radius have high rate of heat transfer.

Table 2. Comparison of $f''(0)$ of the present results (in brackets) with the previous work [36] when $\gamma = 0$, K = 0, and $S = 0$

λ/M	0.0	0.2	0.4	0.6	0.8	1.0
0.0	–1	–0.9131	–0.8452	–0.7906	–0.7454	–0.7071
	(–1)	(–0.91287)	(–0.84516)	(–0.79057)	(–0.74536)	(–0.70711)
0.1	–1	–0.9159	–0.8493	–0.7950	–0.7498	–0.7114
	(–1)	(–0.91590)	(–0.84929)	(–0.79503)	(–0.74979)	(–0.71137)
0.2	–1	–0.9190	–0.8536	–0.7997	–0.7544	–0.7158
	(–1)	(–0.91900)	(–0.85358)	(–0.79968)	(–0.75442)	(–0.71584)
0.3	–1	–0.9222	–0.8580	–0.8045	–0.7593	–0.7205
	(–1)	(–0.92218)	(–0.85804)	(–0.80453)	(–0.75927)	(–0.72048)
0.4	–1	–0.9254	–0.8627	–0.8096	–0.7644	–0.7254
	(–1)	(–0.92543)	(–0.86267)	(–0.80960)	(–0.76436)	(–0.72538)
0.5	–1	–0.9288	–0.8675	–0.8149	–0.7697	–0.7305
	(–1)	(–0.92878)	(–0.86749)	(–0.81493)	(–0.76971)	(–0.73053)
0.6	–1	–0.9322	–0.8725	–0.8205	–0.7754	–0.7360
	(–1)	(–0.93221)	(–0.87252)	(–0.82053)	(–0.77534)	(–0.73598)
0.7	–1	–0.9357	–0.878	–0.8264	–0.7813	–0.7418
	(–1)	(–0.93574)	(–0.87777)	(–0.82643)	(–0.78133)	(–0.74174)
0.8	–1	–0.9394	–0.8833	–0.8327	–0.7877	–0.7479
	(–1)	(–0.93938)	(–0.88327)	(–0.83267)	(–0.78768)	(–0.74788)
0.9	–1	–0.9431	–0.8891	–0.8393	–0.7954	–0.7544
	(–1)	(–0.94312)	(–0.88905)	(–0.83930)	(–0.79446)	(–0.75443)
1.0	–1	–0.9470	–0.8951	–0.8464	–0.8017	–0.7615
	(–1)	(–0.94698)	(–0.89513)	(–0.84637)	(–0.80172)	(–0.76145)

Table 3. Comparison of skin friction coefficient $(\mathrm{Re}_z)^{1/2}Cf$ of the present results (in brackets) with the previous work [36] when $\gamma = 0$, K = 0, and $S = 0$

λ/M	0.0	0.2	0.4	0.6	0.8	1.0
0.0	–1	–1.0954	–1.1832	–1.2649	–1.3416	–1.4142
	(–1)	(–1.09545)	(–1.18322)	(–1.26491)	(–1.34164)	(–1.41421)
0.1	–1	–1.0940	–1.1808	–1.2620	–1.3384	–1.4107
	(–1)	(–1.09395)	(–1.18084)	(–1.26199)	(–1.33838)	(–1.41073)
0.2	–1	–1.0924	–1.1784	–1.2590	–1.3351	–1.4072
	(–1)	(–1.09245)	(–1.17843)	(–1.25902)	(–1.33506)	(–1.40718)
0.3	–1	–1.0909	–1.1776	–1.2560	–1.3317	–1.4036
	(–1)	(–1.09092)	(–1.17598)	(–1.25600)	(–1.33167)	(–1.40356)
0.4	–1	–1.0894	–1.1735	–1.2529	–1.3282	–1.3999
	(–1)	(–1.08938)	(–1.17349)	(–1.25291)	(–1.32821)	(–1.3999)
0.5	–1	–1.0878	–1.1710	–1.2498	–1.3247	–1.3961
	(–1)	(–1.08782)	(–1.17096)	(–1.24976)	(–1.32467)	(–1.39609)
0.6	–1	–1.0862	–1.1684	–1.2466	–1.3211	–1.3922
	(–1)	(–1.08625)	(–1.16838)	(–1.24655)	(–1.32106)	(–1.39223)
0.7	–1	–1.0847	–1.1658	–1.2433	–1.3174	–1.3883
	(–1)	(–1.08465)	(–1.16575)	(–1.24327)	(–1.31736)	(–1.38827)
0.8	–1	–1.0830	–1.1631	–1.2399	–1.3136	–1.3842
	(–1)	(–1.08304)	(–1.16308)	(–1.23991)	(–1.31357)	(–1.38422)
0.9	–1	–1.0814	–1.1603	–1.2365	–1.3097	–1.3801
	(–1)	(–1.08141)	(–1.16035)	(–1.23646)	(–1.30968)	(–1.38006)
1.0	–1	–1.0798	–1.1576	–1.2329	–1.3057	–1.3758
	(–1)	(–1.07975)	(–1.15756)	(–1.23293)	(–1.30569)	(–1.37578)

Conclusions

Here we presented the flow of Powell-Eyring fluid by a stretching cylinder. The HAM is used to find the convergent series solutions of dimensionless momentum and energy equations. Main observations are as follows.

- Fluid parameter increases the velocity while it decreases temperature of the fluid.
- Larger curvature parameter leads to enhancement in both velocity and temperature of the fluid.
- Hartmann number decreases the velocity while it increases temperature of the fluid.
- Magnitude of velocity for Powell-Eyring fluid is greater than viscous fluid for both flat plate and cylinder cases.
- Temperature in viscous fluid is greater than Powell-Eyring fluid for both flat plate and cylinder cases.

Table 4. Numerical values of skin friction for different parameters

M	K^2	γ	$C_f(Re_z)^{1/2}$
0.0	0.1	0.2	0.050318
0.1			0.048337
0.3			0.045014
0.3	0.0	0.2	0.036821
	0.1		0.045014
	0.3		0.052441
0.3	0.1	0.0	0.036719
		0.1	0.041062
		0.2	0.045014

- Higher values of curvature parameter has more rate of heat transfer and thus can be used for the cooling of systems.

Table 5. Numerical values of Nusselt number for different parameters

α	M	ϕ	K	γ	R	Pr	S	$Nu_z(Re_z)^{1/2}$
0.1	0.3	π/3	0.1	0.1	0.2	1.2	0.1	0.3428
0.2								0.3912
0.3								0.4031
0.1	0.0	π/3	0.1	0.1	0.2	1.2	0.1	0.3687
	0.1							0.3968
	0.4							0.3990
0.1	0.3	0.0	0.1	0.1	0.2	1.2	0.1	0.4050
		π/3						0.3899
		π/2						0.3702
0.1	0.3	π/3	0.0	0.1	0.2	1.2	0.1	0.4208
			0.1					0.3852
			0.3					0.3605
0.1	0.3	π/3	0.1	0.0	0.2	1.2	0.1	0.3556
				0.1				0.3968
				0.2				0.4263
0.1	0.3	π/3	0.1	0.1	0.0	1.2	0.1	0.4307
					0.1			0.4275
					0.2			0.4119
0.1	0.3	π/3	0.1	0.1	0.1	0.8	0.1	0.3843
						1		0.4115
						1.2		0.4407
0.1	0.3	π/3	0.1	0.1	0.1	1.2	0.0	0.2430
							0.1	0.2821
							0.2	0.4117

References

[1] Powell, R. E, Eyring, H., Mechanisms for the Relaxation Theory of Viscosity, *Nature*, London, 1944, Vol. 154, pp. 427-428
[2] Patel, M., Timol, M. G., Numerical Treatment of MHD Powell-Eyring Fluid Flow Using the Method of Satisfaction of Asymptotic Boundary Conditions, *International Journal of Mathematics and Computation*, *1* (2011), 2, pp. 71-78
[3] Hayat, T., *et al*., Radiative Effects in a Three-Dimensional Flow of MHD Eyring-Powell Fluid, *Journal of the Egyptian Mathematical Society*, *21* (2013), 3, pp. 379-384
[4] Ara, A., *et al*., Radiation Effect on Boundary Layer Flow of an Eyring-Powell Fluid over an Exponentially Shrinking Sheet, *Ain Shams Engineering Journal*, *5* (2014), 4, pp. 1337-1342
[5] Hayat, T., *et al*., Melting Heat Transfer in the Stagnation Point Flow of PowellEyring fluid, *Journal of Thermophysics and Heat Transfer*, *27* (2013), 4, pp. 761-766
[6] Ishak, A., MHD Boundary Layer Flow Due to an Exponentially Stretching Sheet with Radiation Effect, *Sains Malaysiana*, *40* (2011), 4, pp. 391-395

[7] Noor, N. F. M., Hashim, I., MHD Flow and Heat Transfer Adjacent to a Permeable Shrinking Sheet Embedded in a Porous Medium, *Sains Malaysiana*, *38* (2009), 4, pp. 559-565

[8] Turkyilmazoglu, M., MHD Fluid Flow and Heat Transfer Due to a Shrinking Rotating Disk, *Computers and Fluids*, *90* (2014), Feb., pp. 51-56

[9] Hayat, T., *et al*., MHD Stagnation Point Flow of Second Grade Fluid over a Stretching Cylinder with Heat and Mass Transfer, *International Journal of Nonlinear Sciences and Numerical Simulation*, *15* (2014), 6, pp. 365-376

[10] Sheikholeslami, M., *et al*., Magnetic Field Effect on Nanofluid Flow and Heat Transfer Using KKL Model, *Journal of the Taiwan Institute of Chemical Engineers*, *45* (2014), 3, pp. 795-807

[11] Rashidi, M. M., *et al*., MHD Natural Convection with Convective Surface Boundary Condition over a Flat Plate, *Abstract and Applied Analysis,* Hindawi Publishing Corporation, *2014* (2014), ID 923487

[12] Merkin, J. H., Natural-Convection Boundary-Layer Flow on a Vertical Surface with Newtonian Heating, *International Journal of Heat and Fluid Flow*, *15* (1994), 5, pp. 392-398

[13] Ramzan, M., *et al*., MHD Three-Dimensional Flow of Couple Stress Fluid with Newtonian Heating, *The European Physical Journal Plus*, *128* (2013), 5, pp. 1-15

[14] Salleh, M. Z., Nazar, R., Free Convection Boundary Layer Flow over a Horizontal Circular Cylinder with Newtonian Heating, *Sains Malaysiana*, *39* (2010), 4, pp. 671-676

[15] Salleh, M. Z., *et al*., Numerical Solutions of Free Convection Boundary Layer Flow on a Solid Sphere with Newtonian Heating in a Micropolar Fluid, *Meccanica*, *47* (2012), 5, pp. 1261-1269

[16] Narahari, M., Dutta, B. K., Effects of Thermal Radiation and Mass Diffusion on Free Convection Flow near a Vertical Plate with Newtonian Heating, *Chemical Engineering Communications*, *199* (2012), 5, pp. 628-643

[17] Liao, S., *Homotopy Analysis Method in Non-Linear Differential Equations*, Higher Education Press*,* Bejing, 2012, pp. 153-165

[18] Sajid, M., Hayat, T., The Application of Homotopy Analysis Method for MHD Viscous Flow Due to a Shrinking Sheet, *Chaos, Solitons & Fractals*, *39* (2009), 3, pp. 1317-1323

[19] Abbasbandy, S., Shirzadi, A., Homotopy Analysis Method for Multiple Solutions of the Fractional Sturm-Liouville Problems, *Numerical Algorithms*, *54* (2010), 4, pp. 521-532

[20] Liao, S. J., On the Homotopy Multiple-Variable Method and Its Applications in the Interactions of Nonlinear Gravity Waves, *Communications in Nonlinear Science and Numerical Simulation*, *16* (2011), 3, pp. 1274-1303

[21] Abbasbandy, S., *et al*.,The Homotopy Analysis Method and the Linard Equation, *International Journal of Computer Mathematics*, *88* (2011), 1, pp. 121-134

[22] Rashidi, M. M., *et al*., A Study of Non-Newtonian Flow and Heat Transfer over a Non-Isothermal Wedge Using the Homotopy Analysis Method, *Chemical Engineering Communications*, *199* (2012), 2, pp. 231-256

[23] Shahzad, A., Ali, R., Approximate Analytic Solution for Magneto-Hydrodynamic Flow of a Non-Newtonian Fluid over a Vertical Stretching Sheet, *Can. J. Appl. Sci.*, *2* (2012), Jan., pp. 202-215

[24] Sheikholeslami, M., *et al*., Investigation of the Laminar Viscous Flow in a Semi-Porous Channel in the Presence of Uniform Magnetic Field Using Optimal Homotopy Asymptotic Method, *Sains Malaysiana*, *41* (2012), 10, pp. 1177-1229

[25] Masood, K., *et al*., MHD Falkner-Skan Flow with Mixed Convection and Convective Boundary Conditions, *Walailak Journal of Science and Technology*, *10* (2013), 5, pp. 517-529

[26] Khan, J. A., *et al*., On Model for Three-Dimensional Flow of Nanofluid: An Application to Solar Energy, *Journal of Molecular Liquids*, *194* (2014), June, pp. 41-47

[27] Aziz, T., *et al*., Travelling Wave Solutions for the Unsteady Flow of a Third Grade Fluid Induced Due to Impulsive Motion of Flat Porous Plate Embedded in a Porous Medium, *Journal of Mechanics*, *30* (2014), 5, pp. 527-535

[28] Hayat, T., *et al*., Thermally Stratified Stagnation Point Flow of an Oldroyd-B Fluid, *International Journal of Nonlinear Sciences and Numerical Simulation*, *15* (2014), 1, pp. 77-86

[29] Ali, R., *et al*., Analytic and Numerical Solutions for Axisymmetric Flow with Partial Slip, *Engineering with Computers*, *32* (2016), 1, pp. 149-154

[30] Hayat, T., *et al*., Magnetohydrodynamic Flow by a Stretching Cylinder with Newtonian Heating and Homogeneous-Heterogeneous Reactions, *PloS One*, *11* (2016), 6, e0156955

[31] Hayat, T., *et al*., Heterogeneous-Homogeneous Reactions and Melting Heat Transfer Effects in Flow with Carbon Nanotubes, *Journal of Molecular Liquids*, *220* (2016), Aug., pp. 200-207

[32] Hayat, T., *et al*., Stagnation Point Flow with Cattaneo-Christov Heat Flux and Homogeneous-Heterogeneous Reactions, *Journal of Molecular Liquids*, *220* (2016), Aug., pp. 49-55
[33] Hayat, T., *et al*., Impact of Cattaneo-Christov Heat Flux Model in Flow of Variable Thermal Conductivity Fluid over a Variable Thicked Surface, *International Journal of Heat and Mass Transfer*, *99* (2016), Aug., pp. 702-710
[34] Hayat, T., *et al*., Carbon Nanotubes Effects in the Stagnation Point Flow Towards a Non-Linear Stretching Sheet with Variable Thickness, *Advanced Powder Technology*, *27* (2016), 4, pp. 1677-1688
[35] Khan, M. I., *et al*., Numerical Investigation of Magnetohydrodynamic Stagnation Point Flow with Variable Properties, *Alexandria Engineering Journal*, *55* (2016), 3, pp. 2367-2373
[36] Javed, T., *et al*., Flow of an Eyring-Powell Non-Newtonian Fluid over a Stretching Sheet, *Chemical Engineering Communications*, *200* (2013), 3, pp. 327-336

Paper submitted: July 17, 2015
Paper revised: June 27, 2016
Paper accepted: June 30, 2016